Acoustic Analysis of Viscous Fluid Ejection Using Ultrasonic Atomizer

D.A. Loney, W. Zhou, D.W. Rosen, F.L. Degertekin, A.G. Fedorov
Georgia Institute of Technology
813 Ferst Drive, Atlanta, GA, 30332-0405

Reviewed, accepted September 23, 2010

Abstract

The acoustics of the Additive Manufacturing via Microarray Deposition (AMMD) system based on a ultrasonic atomizer is investigated for printing high viscosity fluids for 3D inkjet manufacturing applications. The ultrasonic atomizer incorporates a piezoelectric transducer, a material reservoir, and a silicon micromachined array of acoustic horn structures as ejection nozzles. When driven at the resonance frequencies of the fluid cavity, the nozzle geometry focuses the acoustic waves resulting in a locally increased pressure gradient at the nozzle apex. Previously, AMMD has demonstrated successful ejection of fluids with viscosity as high as 3000 mN-s/m^2, overcoming the viscosity limitations traditionally associated with piezoelectric droplet formation. However, the physics of ejection of such high-viscosity fluids is not well understood. This work focuses on understanding the acoustics of the AMMD system through complimentary simulations and experimental characterization. Specifically, ANSYS finite element software was used to model acoustic wave attenuation due to viscosity inside the material cavity and its implication on the pressure gradient at nozzle apex, which drives the fluid ejection. Additionally, the affect of fluid attenuation on cavity resonance modes, both the frequency and the quality factor, is characterized for fluids of a large variation range in viscosity. Finally, preliminary guidelines for improved design and efficient operation of the AMMD system are formulated based on an insight into a device's acoustic behavior with high viscosity fluids.

Introduction

Ink-jet printing produces droplets from a fluid reservoir and directs the impact of those droplets onto a substrate. Expertise developed in controlling droplet generation and impact make ink-jet processes ideal for additive manufacture (AM) applications.[1] Moreover, AM via ink-jet printing provides significant benefits over other AM techniques through scalability, low cost, and simultaneous deposition of multiple materials. Despite these benefits, AM via ink-jet printing has found limited usage due to fluid physical constraints on droplet generation, such as viscosity, surface tension, and other complex rheological behavior.[2] Of particular interest is printing of high viscosity fluids, which present a fundamental challenge of ejectability under moderate operating temperatures.

Recent efforts have sought to expand the types of fluids that can be printed for AM applications beyond current viscosity limitations. Wilkes et al. examined viscous droplet generation from a print nozzle using a capillary tube and applying a constant pressure to achieve ejection.[3] Xu and Basaran expanded this initial analysis to a sinusoidal driving force, again with capillary tube and with focus primarily on filament length as a function of viscosity.[4] In addition, slurries, powder melts, and gels have been experimentally investigated for their printability.[5-8] Despite these efforts, the choice of materials with AM continues to be limited by the ability to produce droplets either directly from the print head or from jet breakup.

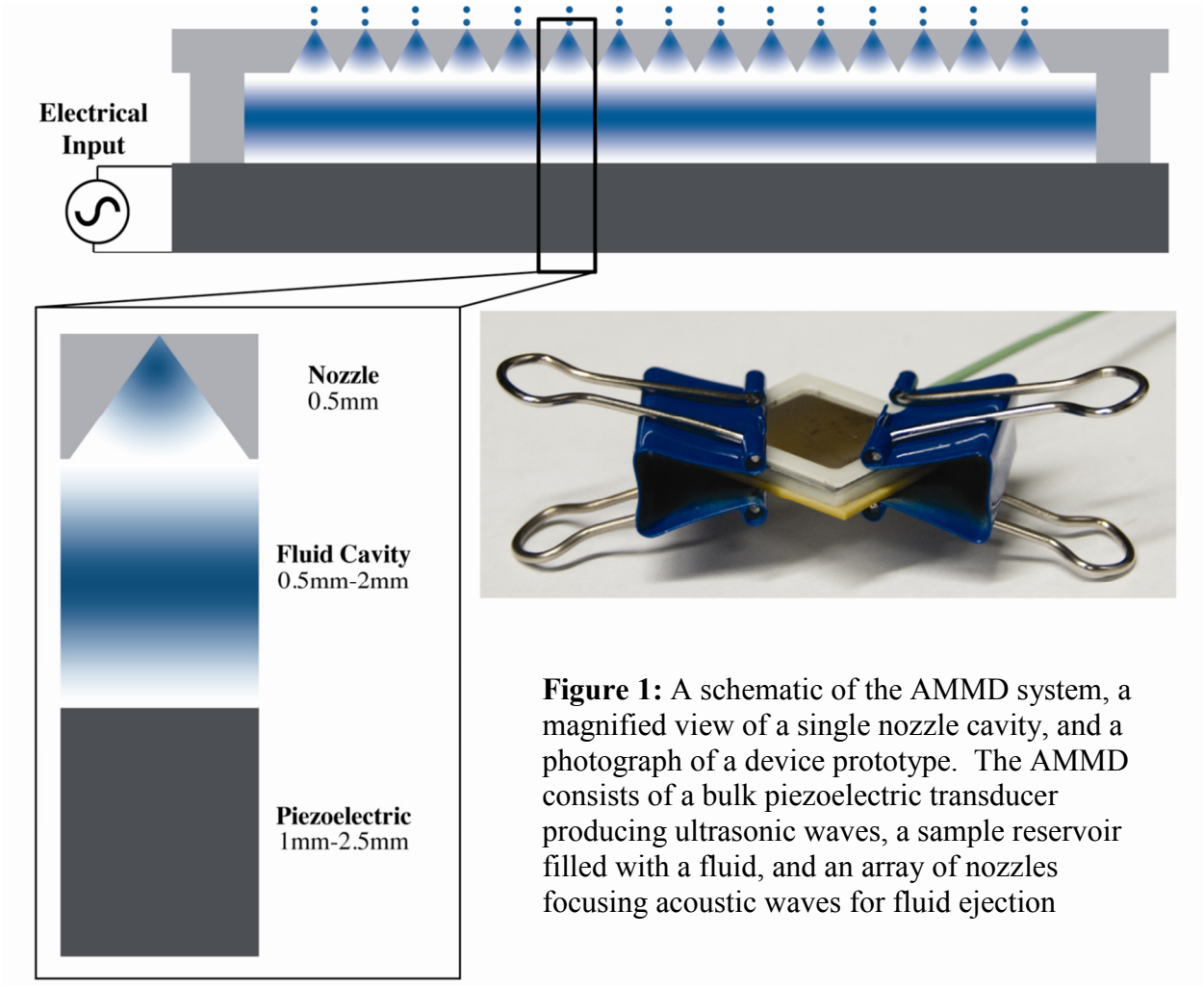

Figure 1: A schematic of the AMMD system, a magnified view of a single nozzle cavity, and a photograph of a device prototype. The AMMD consists of a bulk piezoelectric transducer producing ultrasonic waves, a sample reservoir filled with a fluid, and an array of nozzles focusing acoustic waves for fluid ejection

Fluid properties relevant to printability – namely viscosity (μ), surface tension (σ), and density (ρ) – are bundled into a non-dimensional printing indicator:

$$Z = \frac{\sqrt{\rho\sigma L}}{\mu} \tag{1}$$

which is the inverse of the Ohnesorge number.[9, 10] Fromm initially showed numerically that Z must generally be greater than 2 for fluid printability, while Jang et al. most recently proposed a revision of the bounds upward to $4 < Z < 14$ by defining material printability to minimize the formation of smaller, unwanted satellite droplets.[2, 11] Within systems utilizing acoustic waves for droplet generation, pressure wave attenuation due to viscous energy dissipation defines the lower boundary for printing and satellite droplet formation establishes the upper limit. As fluid attenuation is proportional to viscosity, viscosity largely determines the lower threshold on printability. More generally, the accepted range for successful fluid printing is taken to be $1 < Z < 10$, though these bounds are not derived based on first principles and therefore may be further adjusted with new systems and printing techniques.

The Additive Manufacturing via Microarray Deposition (AMMD) system (Figure 1) consists of a piezoelectric transducer capable of generating the ultrasonic waves, a sample

reservoir filled with the fluid to be ejected, and an array of pyramidal nozzle micromachined in silicon acting as the acoustic wave focusing horns. When the device operates at a resonant frequency of the nozzles and fluid cavity, the acoustic horns amplify the pressure gradient locally near the nozzle orifice resulting in an efficient means for fluid ejection. Typical device operation is in the range between 0.5 and 3.5 MHz, adjustable based on the ejector geometry, and results in either droplet-mode or jet-mode ejection based on orifice size and physical properties of the fluid.[12] Scalability is achieved by using multiple print head arrays, adjusting the number of active nozzles within each array, or by multiplexed operation of the device.[13] The AMMD system has successfully ejected fluids with viscosity as great as 3000 mN-s/m^2, albeit only for short time periods at the higher range of viscosities, giving a printing indicator of approximately 0.01.[14]

While the capability to eject high viscosity fluids has been demonstrated by the AMMD apparatus, the basic acoustics and fluid mechanics underlying the ejection process for such fluids has not been fully characterized. To this end, this paper focuses on acoustic behavior and examines the affect of ultrasonic pressure wave attenuation on the performance of the ultrasonic atomizer. This is done through a combination of numerical simulations and experiments to investigate the effect of viscous wave attenuation in the fluid on the ejection pressure gradient for different device geometries. Resulting understanding is relevant to developing guidelines for improved design and operation of the AMMD system using engineering fluids with the viscosity in the range relevant to AM applications.

Model Implementation

ANSYS Mechanical (ANSYS) is a commercially available, finite element software package designed to solve problems involving coupled physics.[15] ANSYS includes the capability to simulate acoustic wave propagation in a coupled fluid reservoir, nozzle plate, and piezoelectric transducer domains, allowing the full atomizer to be modeled in a single computational domain. Pre-programmed element types provide the basis for model construction and incorporating material behavior.

The piezoelectric transducer is modeled as an APC International 855 material modeled with Plane13 elements.[16] The fluid reservoir is formed by the spacer frame placed on either edge of the piezoelectric actuator and is modeled as acoustically lossless silicon having a Young's modulus of 150 GPa, a Poisson's ratio of 0.21, and a density of 2330 kg/m^3 with element type of Plane82. The nozzle array is made of the same silicon material as the spacer and is modeled with the same element.

Fluid29 is the standard fluid element for acoustic analysis within ANSYS. The mesh topology supporting Fluid29 are quadrilaterals which allow degeneration to triangles, containing two-dimensional displacement and pressure variables as degrees of freedom. This element includes interfacial damping at fluid structure boundaries, but assumes inviscid behavior throughout the bulk material and therefore cannot be used for viscous damping of acoustic waves.

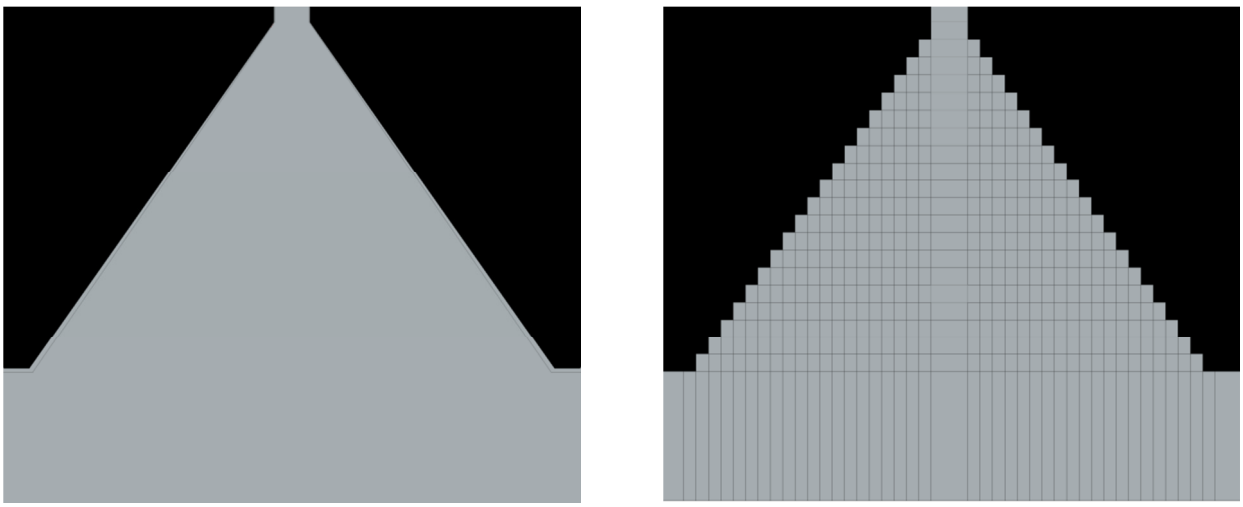

Figure 2: Nozzle geometry for the a) Fluid29 and the b) Fluid79 models. Due to the limitation on the Fluid 79 element to a rectangular shape, the nozzle slope requires division into a series of steps.

Fluid79, a secondary acoustic fluid element, incorporates damping in the bulk material but presents functional limitations on implementation. Shape is constrained as rectangular with two displacement degrees of freedom. The shape constraint limits the geometry that can be meshed; any significant slope cannot be directly meshed with Fluid79. Furthermore, any deviation from a rectangular shape rapidly introduces numerical error. Relevant material properties for this element are the bulk modulus and density, from which then ANSYS calculates the adiabatic speed of sound.

Fluid79 discretizes the domain using structural mechanics formalism, as it is remapped from structural element Plane42. Beginning with the matrix form of the stress-strain relationship:

$$\{\sigma\} = D\{\varepsilon^{el}\} \tag{2}$$

where σ is the stress tensor, D is the bulk modulus for a fluid, and ε^{el} is the strain tensor in the element, one can apply the principle of virtual work to obtain:

$$[M_e]\{\ddot{u}\} + [C]\{\dot{u}\} - \left([K_e] + \left[K_e^f\right]\right)\{u\} = -(\{F_e^{th}\} + \{F_e^{pr}\} + \{F_d^{nd}\}) \tag{3}$$

where u is the element displacement, M_e is the element mass matrix, C is the element damping matrix, K_e is the element stiffness matrix, K_e^f is the element foundation stiffness matrix, F_e^{th} is the thermal load vector, F_e^{pr} is the element pressure vector, and F_d^{nd} are the nodal forces applied to the element. The element damping matrix takes the form of:

$$[C] = \alpha[M] + (\beta + \beta_c)[K] + \sum_{j=1}^{N_m}\left[\left(\beta_j^m + \left(\frac{2}{\Omega}\right)\beta_j^\zeta\right)[K_j]\right] + \sum_{k=1}^{N_e}[C_k] + [C_\zeta] \tag{4}$$

α: mass matrix multiplier
$[M]$: mass matrix
β: stiffness multiplier
β_c: variable stiffness multiplier
$[K]$: stiffness matrix
N_m: number of materials with damping in the domain
β_j^m: stiffness matrix multiplier for material j
β_j^ζ: frequency independent matrix coefficient for material j
Ω: angular frequency
K_j: portion of the structure stiffness matrix for material j
N_e: number of elements with a given damping value
C_k: element damping matrix
C_ζ: frequency dependent damping matrix

For a harmonic analysis with Fluid79, all terms other than β_c are generally zero. β_c represents a nondimensional ratio between actual damping and critical damping within the fluid, expressed by nondimensionalizing α_s as α_s/k, where α_s is the spatial attenuation coefficient and k is the wavenumber. The nondimensionalization can be readily obtained from common wave dispersion relations.[17] Attenuation is typically provided as a frequency (f) independent value, α_s/f^2 which grows linearly proportional to viscosity.

Figure 2 shows the nozzle geometry utilized with each type of fluid element. Figure 2a), meshed with Fluid29, reflects the actual geometry of the nozzle by incorporating sloped nozzle sides without approximation, as allowed by the element's ability to conform to the slope. Figure 2b), meshed with Fluid79, utilizes a stepped approximation of the nozzle side wall geometry to allow meshing with Fluid79 elements. For full device simulations an array of nine nozzles is analyzed. It should be noted that the analysis performed is limited to 2D representation of the actual 3D shape, due to limitations imposed by the computer memory requirements for simulations. The pressure release boundary condition is used at the nozzle apex, and 10V AC signal is used to drive the piezoelectric transducer.

To ensure the models produced similar results, the pressure distribution along the center nozzle with the physically accurate (sloped), Fluid29 nozzle geometry was compared to the simulation results using both Fluid29 and

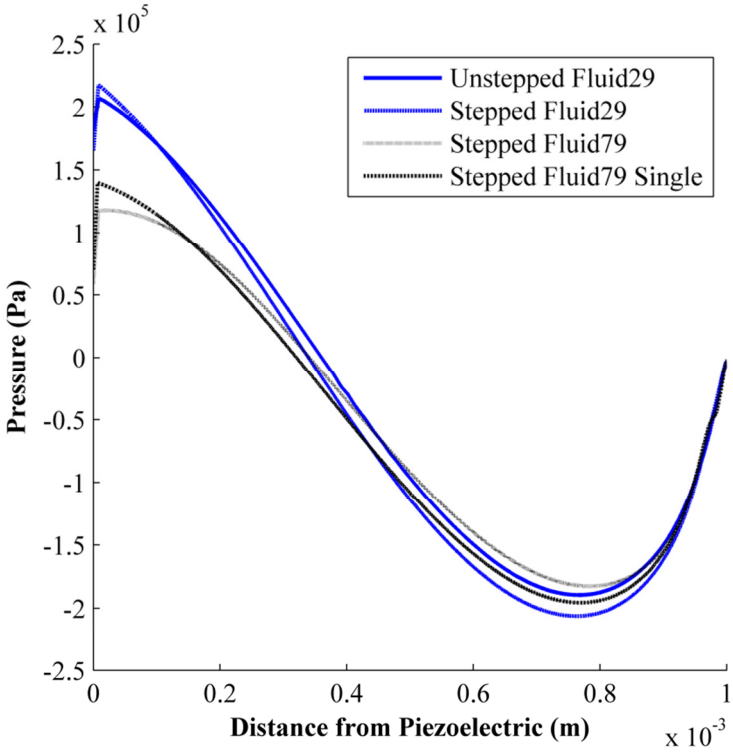

Figure 3: Comparison of the pressure distributions along the center nozzle for the first nozzle mode of glycerol with zero attenuation and a 0.5mm spacer obtained using different ANSYS elements and domain discretization methods.

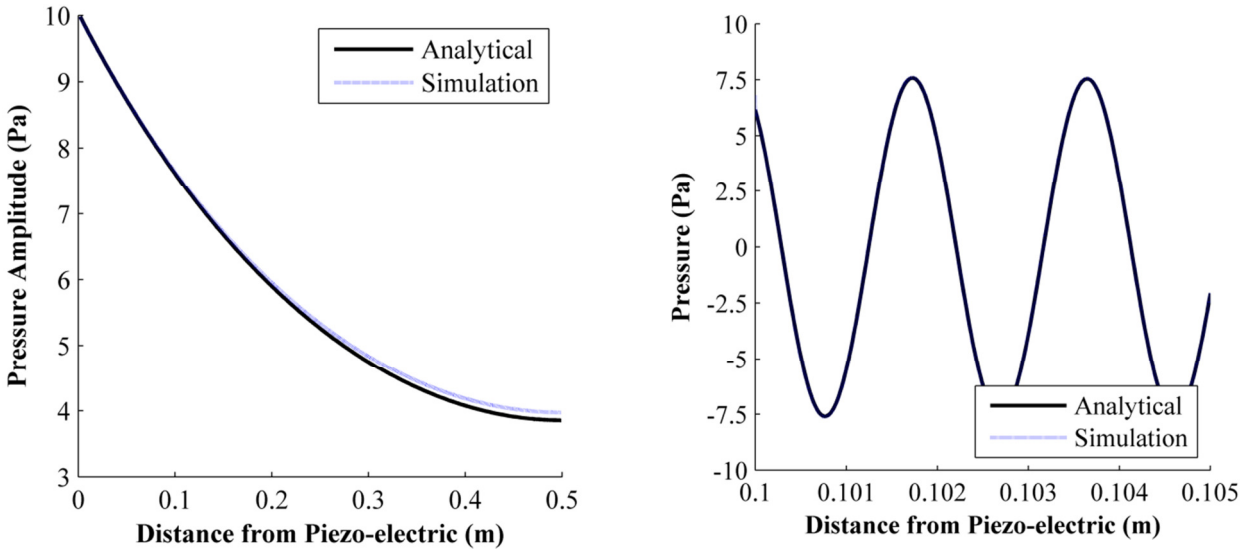

Figure 4: (a) Decay in the amplitude of the pressure wave propagating along a 0.5m glycerol tube, as driven at the inlet by a harmonically-oscillating pressure of 10 Pa amplitude and having a fixed end condition. (b) A snapshot of the waveform near the 0.1m away from the inlet of the tube. The analytical and Fluid79 simulation results essentially overlap, showing an excellent agreement

Fluid79 elements with the stepped nozzle for the zero attenuation case (Figure 3). A good qualitative and quantitative agreement between simulation results with the Fluid29 element for the unstepped and stepped simulation domain support the applicability of the approximate, stepped geometry with sufficiently fine steps to predict wave propagation in the nozzle horn. The comparable result between the stepped Fluid29 and Fluid79 models, particularly near the nozzle apex which is of the most interest, validates the use of the Fluid79 element. Additionally, a unit cell model for a single nozzle was developed for the Fluid79 nozzle geometry, aiming at increasing the speed of simulations. As shown in Figure 3, the single nozzle Fluid79 simulation predicts a pressure distribution closely resembling that for the Fluid79 element simulations of the full array, thus justifying its use for computationally-demanding parametric simulations.

In all simulations, convergence was assumed when further mesh refinement resulted in less than 1% change in the pressure magnitude at the central nozzle in the array. Simulations were sensitive to element size and distribution, requiring a gradual decrease in element size near the nozzle walls. Models utilizing the Fluid79 element were also intolerant of any deviation from a rectangular shape.

Results and Discussion

The capability of Fluid79 element to simulate damping behavior was first confirmed analytically by simulating a wave propagating in a one-dimensional glycerol tube, results of which are shown in Figure 4. Relative error from analytical values was determined to be an acceptable 0.612% for the glycerol and as low as 0.053% for water under similar conditions, supporting the ability of the Fluid79 element to accurately incorporate attenuation into acoustic analysis.

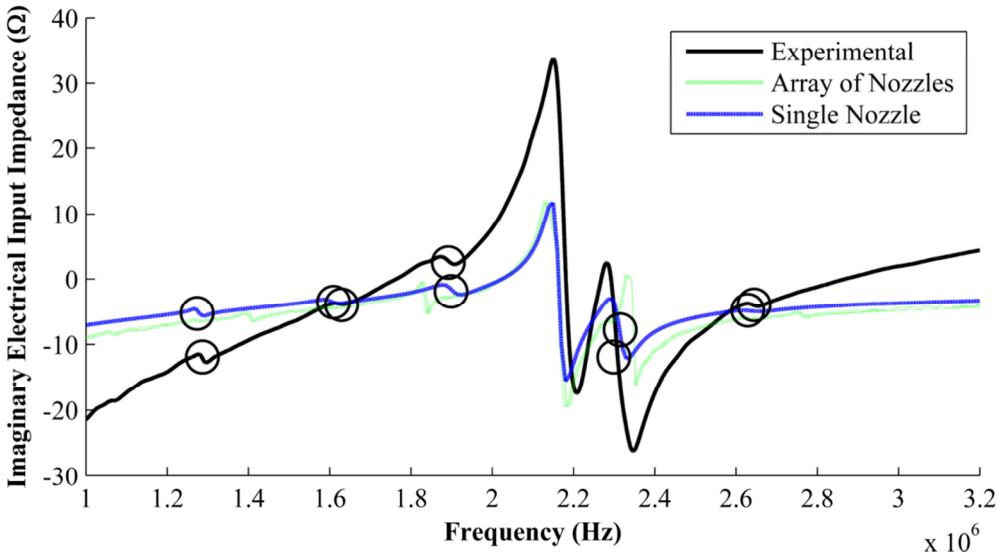

Figure 5: Electrical input impedance as a function of frequency for a device with 2.1 mm reservoir height loaded with glycerol and driven by a 1mm piezoelectric transducer comparing the resonant modes of the experiment and simulations.

The capability of simulations using Fluid79 element to accurately predict device resonances was confirmed using the experimentally measured electrical input impedance (Agilent 8753ES Network Analyzer) of a device loaded with glycerol. The tested device had a reservoir with a height of 2.1mm and was driven by a 1 mm thick piezoelectric transducer (APC International 855). Figure 5 compares the measurements to simulation values as a function of frequency, with the nozzle resonant modes circled. Though the simulation of the nozzle array does show a slight frequency shift in the nozzle resonant frequency, most likely due to the limited number of nozzles simulated (9 as compared to 15 in the tested device), the single nozzle results closely agree with the experimentally measured resonant frequencies when normalized by the ratio of single nozzle simulation piezoelectric area to the piezoelectric area of the experimental device. The simulations also accurately capture the relative quality of different resonance modes. The quantitative differences reflect the fact that there are geometric (e.g., 2D simulations vs. 3D test device) and boundary condition differences between the model setup and a prototype package used in experiments. Overall, favorable comparison between predictions and measurements provides validation of the ANSYS model developed in respect to proper coupling between the Fluid79 elements and the transducer as well as our methodology for incorporating the wave attenuation in a lossy fluid.

Figures 3 and 5 demonstrate that the resonant frequencies and pressure distributions of the single nozzle simulation closely match those of the nozzle array simulation, thus supporting the use of the single nozzle model for faster, yet accurate simulations of the multi-nozzle device. Therefore, all parametric simulations reported in the following sections have been performed using a single nozzle model of the device with the Fluid79 element.

Effects of Wave Attenuation in a Lossy Fluid

To assess if viscous attenuation has an effect on the fluid cavity resonance modes, shifts in nozzle resonant frequency were determined using a “test fluid” with acoustic properties of

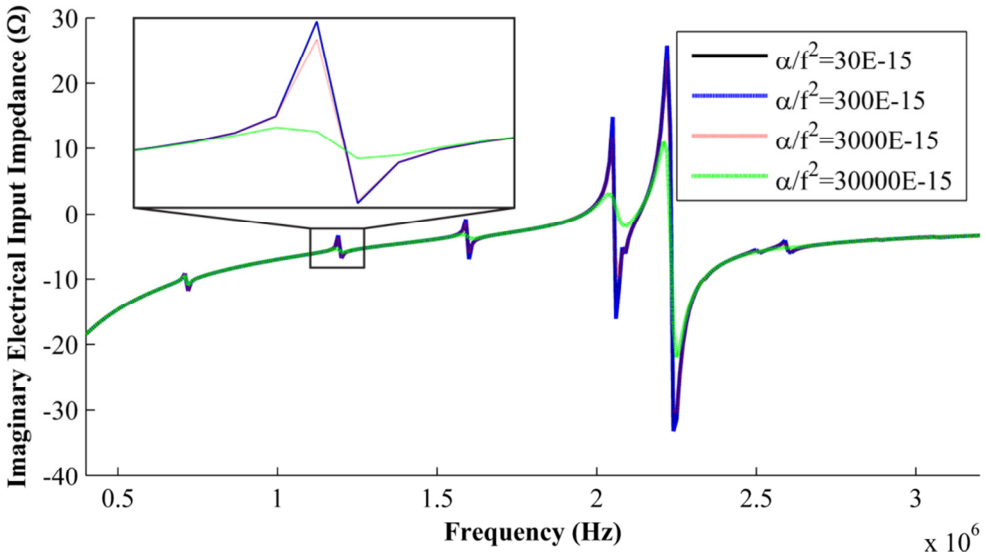

Figure 6: Electric input impedance as a function of frequency assuming water properties but with artificially increased attenuation with a fluid reservoir and transducer thicknesses of 1mm each

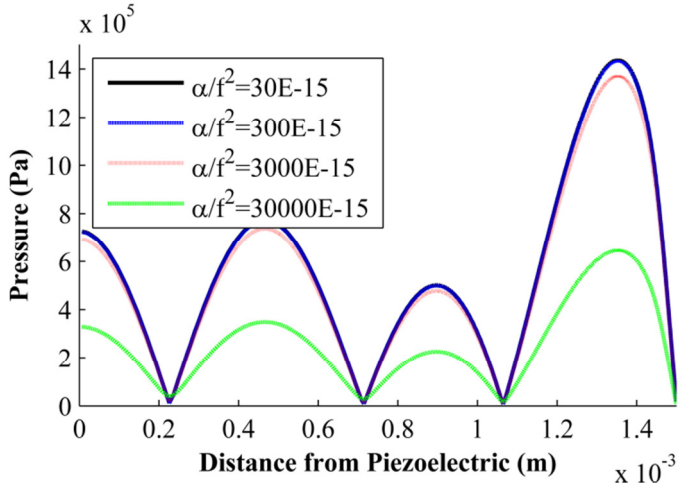

Figure 7: Pressure magnitude assuming water properties with increasing damping values for a device with 2.1 mm reservoir height loaded with glycerol and driven by a 1mm piezoelectric transducer

water but with artificially increased values of attenuation for a fixed device geometry. Attenuation was varied from $\alpha/f^2 = 30 \times 10^{-15}$ per meter, corresponding to water, to $\alpha/f^2 = 30000 \times 10^{-15}$per meter, an order of magnitude greater than glycerol. As Figure 6 demonstrates, the resonant frequencies of the device appear to be independent of the magnitude of the attenuation parameter.

Figure 7 shows the standing pressure wave distribution along the centerline of the fluid reservoir and the nozzle cavity, as a function of the attenuation coefficient. The results indicate that attenuation parameter smaller than $\alpha/f^2 = 30000 \times 10^{-15}$ per meter causes only small pressure amplitude reductions due to the short path that a wave travels within the device fluid

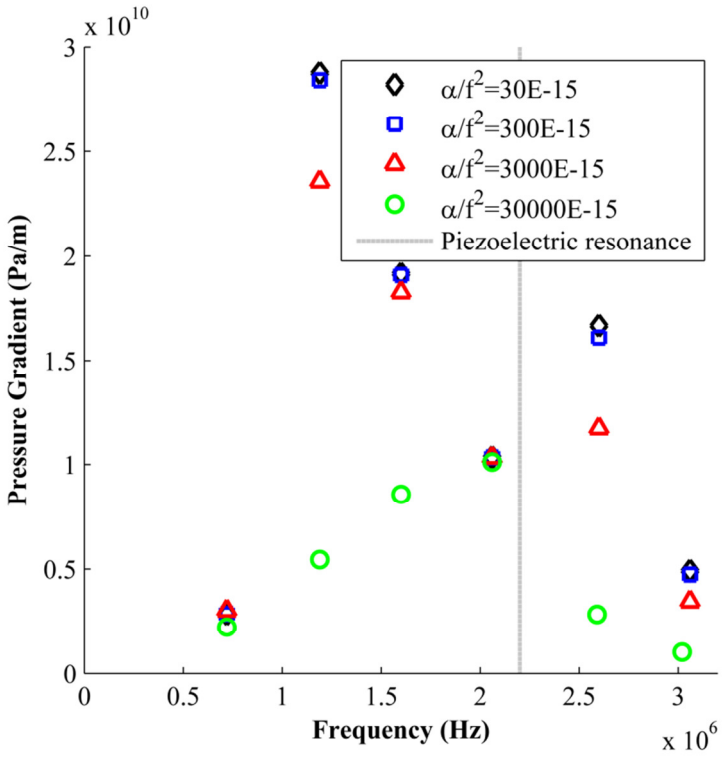

Figure 8: Pressure gradient at the nozzle apex as a function of resonant frequency, assuming water properties and increasing values of attenuation.

cavity. For higher values of α_s/f^2, pressure amplitude reduction becomes significant but focusing behavior of the acoustic horn formed by the nozzle structure remains present with an amplified pressure gradient at the nozzle apex near fluid ejection point.

The driving mechanism for fluid ejection is the pressure gradient generated at the nozzle apex, shown in Figure 8 as a function of the attenuation parameter. Although there is a significant difference in the pressure gradient among different resonant modes of the device, for low values of α_s/f^2, the pressure gradient for each resonant mode changes little, owing to a short path for wave propagation within the cavity. As the attenuation parameter increases, the pressure gradient becomes reduced for all modes, except the first, fundamental cavity mode (~0.7 MHz) and the mode (~2.1 MHz) closest to the piezoelectric transducer's resonance (~2.2 MHz). It is interesting to note that modes whose frequency is lower than the transducer resonance generally yield a greater pressure gradient than modes whose frequency is greater than the transducer resonance.

Effects of Device Geometry

Figures 9 and 10 display the effect of changing the fluid reservoir height on the pressure gradient at the nozzle apex for glycerol and water, respectively. As expected, the magnitude of the pressure gradient is much greater across all the modes for a less lossy fluid (water) as compared to more viscous glycerol. Glycerol also shows a distinct trend of increased pressure gradients for resonant modes occurring near the piezoelectric transducer resonance. In contrast, water displays a more uniform pressure gradient across all resonant modes, with an elevated pressure gradient for certain modes with no particular dependence on the location with respect to

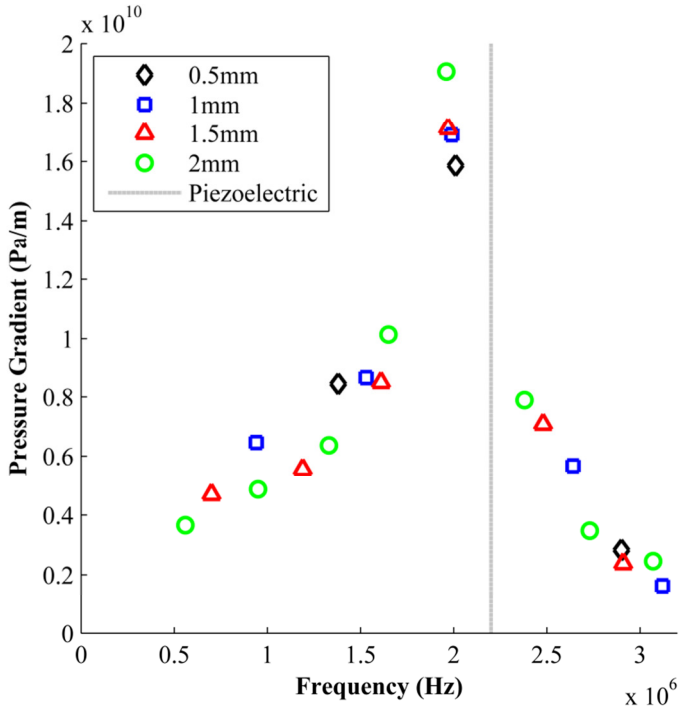

Figure 9: Pressure gradient at the nozzle apex as a function of resonant frequency for various fluid reservoir heights, assuming glycerol properties ($\boldsymbol{\alpha/f^2 = 3000 \times 10^{-15}}$ per meter) and a 1mm thick transducer

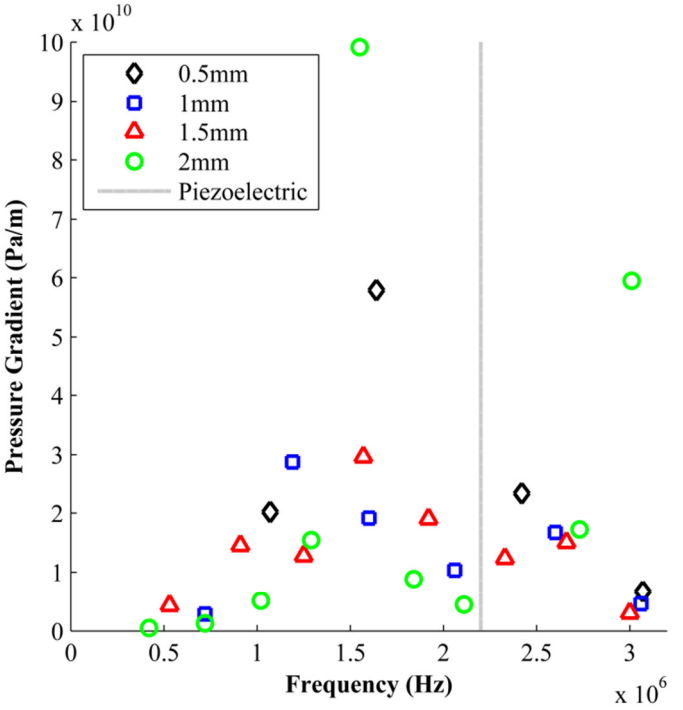

Figure 10: Pressure gradient at the nozzle apex as a function of resonant frequency for various fluid reservoir heights, assuming water properties ($\boldsymbol{\alpha/f^2 = 25 \times 10^{-15}}$ per meter) and a 1mm thick transducer

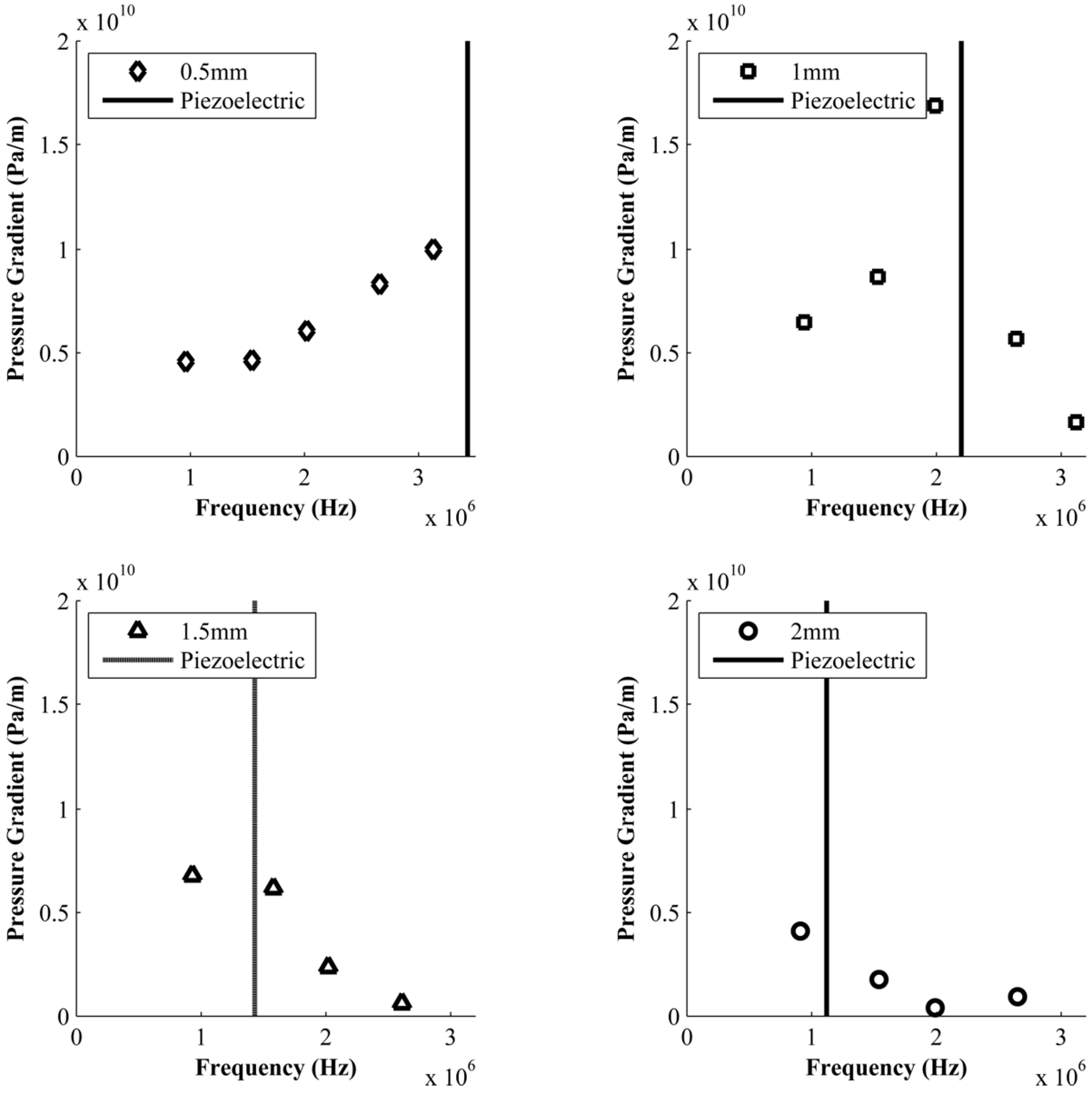

Figure 11: Pressure gradient at the nozzle apex as a function of resonant frequency for various transducer thicknesses, assuming glycerol properties and a reservoir height of 1mm

the transducer resonance. The magnitude of the pressure gradient for both fluids is largely independent of the fluid reservoir height and can be targeted by selecting an ejection mode at a fixed fluid height. Moreover, the dependence of the glycerol pressure gradient on the transducer resonant frequency implies one may vary both ejection mode and the transducer height/material to obtain an optimal pressure gradient for ejection. However, the lack of such dependence in water indicates that device dimension changes may have limited effect for low viscosity fluids where the pressure wave attenuation due to attenuation is less between resonant modes.

Figure 10 further examines the dependence of the pressure gradient at the nozzle apex on the transducer resonant frequency. The transducer resonant frequency is adjusted by increasing

the thickness of the material, from 0.5 mm to 2 mm, lowering its resonant frequency. In general, as the transducer resonant frequency shifts, the fluid cavity modes nearest the transducer frequency always yield the largest pressure gradients. However, those cavity modes near the transducer frequency do not attain equal magnitude for all transducer frequencies. For example, the third cavity mode at ~2 MHz frequency for 1 mm thick fluid reservoir driven by a 1 mm piezoelectric transducer yields a pressure gradient almost twice as large as all other cases. This leads to the conclusion than an optimal piezoelectric transducer resonance frequency exists for a given fluid and fluid reservoir height such as to produce a maximum pressure gradient at the ejection point. Performing such an optimization would be critical for printing high viscosity fluids where maximizing the pressure gradient is of the paramount importance to achieve ejectability.

Conclusion

Droplet generation from high viscosity (low printing indicator) fluids continues to be a challenge for AM applications. The AMMD system based on an ultrasonic atomizer has shown the ability to print fluids with significantly greater viscosity that traditional ink-jet based methods, but optimization of device design for stable, sustained operation requires an in-depth understanding of physical fields underlying fluid ejection. This paper focuses on the development of simulation tools and the prediction of an acoustic field in the ultrasonic atomizer with a particular emphasis placed on accounting for the pressure wave attenuation by highly viscous fluids. The standard ANSYS Fluid79 element has been shown to be capable of incorporating attenuation into an acoustic analysis. Through the incorporation of attenuation, it has been shown that increased attenuation does not affect the AMMD nozzle resonant frequency, given that other fluid properties are held constant. Furthermore, for varying fluid cavity heights of water and glycerol – two model fluids having properties representative of many materials of interest to AM applications – the pressure gradient has been shown to be largely independent of fluid attenuations values for a fixed ejector geometry. Finally, it has been shown that by adjusting the fluid reservoir height and the piezoelectric transducer resonant frequency, one can optimize the apparatus to yield a maximum in the pressure gradient, facilitating the printing of traditionally unprintable materials.

Acknowledgements

We would like to express our appreciation to the National Science Foundation for award DMI-0900322 which supports our work. Any opinions, findings, and conclusions or recommendations expressed in this publication are those of the authors and do not necessarily reflect the views of the National Science Foundation. We would also like to express our gratitude to Dr. J. Mark Meacham for his assistance with simulations and experiments discussed in this paper.

Bibliography

1. Calvert, P., *Inkjet printing for materials and devices.* Chemistry of Materials, 2001. **13**(10): p. 3299-3305.
2. Jang, D., D. Kim, and J. Moon, *Influence of Fluid Physical Properties on Ink-Jet Printability.* Langmuir, 2009. **25**(5): p. 2629-2635.
3. Wilkes, E.D., S.D. Phillips, and O.A. Basaran, *Computational and experimental analysis of dynamics of drop formation.* Physics of Fluids, 1999. **11**(12): p. 3577.

4. Xu, Q. and O.A. Basaran, *Computational analysis of drop-on-demand drop formation.* Physics of Fluids, 2007. **19**(10).
5. Ainsley, C., N. Reis, and B. Derby, *Freeform fabrication by controlled droplet deposition of powder filled melts.* Journal of Materials Science, 2002. **37**(15): p. 3155-3161.
6. Gepp, M.M., et al., *Dispensing of very low volumes of ultra high viscosity alginate gels: a new tool for encapsulation of adherent cells and rapid prototyping of scaffolds and implants.* Biotechniques, 2009. **46**(1): p. 31-+.
7. Sukeshini, A.M., et al., *Inkjet Printing of Anode Supported SOFC: Comparison of Slurry Pasted Cathode and Printed Cathode.* Electrochemical and Solid State Letters, 2009. **12**(12): p. B176-B179.
8. *High-viscosity inkjet prints many materials simultaneously.* Advanced Materials & Processes, 2008. **166**(2): p. 18-18.
9. Derby, B., Reis, N., Seerden, K.A.M., Grant, P.S., Evans, J.R.G., *Freeform Fabrication of Ceramics by Hot-Melt Ink-Jet Printing.* Proceedings of the Materials Research Society, 2000. **625**.
10. Seerden, K.A.M., et al., *Ink-jet printing of wax-based alumina suspensions.* Journal of the American Ceramic Society, 2001. **84**(11): p. 2514-2520.
11. Fromm, J.E., *Numerical calculation of the fluid dynamics of drop-on-demand jets.* IBM J. Res. Dev., 1984. **28**(3): p. 322-333.
12. Meacham, J.M., et al., *Droplet formation and ejection from a micromachined ultrasonic droplet generator: Visualization and scaling.* Physics of Fluids, 2005. **17**(10).
13. Forbes, T.P., F.L. Degertekin, and A.G. Fedorov, *Multiplexed operation of a micromachined ultrasonic droplet ejector array.* Review of Scientific Instruments, 2007. **78**(10).
14. Meacham, J.M., et al., *Micromachined Ultrasonic Print-Head for Deposition of High-Viscosity Materials.* Journal of Manufacturing Science and Engineering-Transactions of the Asme, 2010. **132**(3).
15. ANSYS Inc. 2010 [cited 2010 July 2]; Available from: http://www.ansys.com/.
16. APC International. *APC International, Ltd.* 2009 [cited 2010 July 2]; Available from: http://www.americanpiezo.com/.
17. Blackstock, D.T., *Fundamentals of Physical Acoustics*. 1 ed. 2000: Wiley & Sons Inc.